Tunable charge injection from graphene to halide perovskite induced by reversible ion segregation

Shanika Wanigasekara,[1] Ghadah Alkhalifah,[1,2] Bhupal Kattel,[1] and Wai-Lun Chan[1,*]
[1]*Department of Physics and Astronomy, University of Kansas, Lawrence, Kansas 66045, USA*
[2]*Department of Physics, College of Science, King Faisal University, Al-Ahsa 31982, Saudi Arabia*

(Received 2 May 2023; accepted 1 June 2023; published 15 June 2023)

Migration of point defects can result in various performance instabilities in organometal halide perovskite devices. In particular, the segregation of charged defects can influence the electron transport, but the correlation between ionic and electronic transports remains elusive. In this work, we use a graphene/methylammonium lead iodide capacitor to probe the effect of ion segregation on the charge injection behavior at the graphene/perovskite junction. In our samples, the ion segregation in the perovskite film is induced by a controllable electric field applied through an electrostatic gate. At the same time, the charge injection from graphene to the perovskite is probed by monitoring changes in the graphene conductivity. It is found that a positive (negative) defect accumulation layer near the graphene/perovskite interface can facilitate electron (hole) injection from the graphene electrode to the perovskite. Because the polarity of the defect accumulation layer is switchable by changing the direction of the applied electric field, the graphene/perovskite interface behaves like a Schottky junction with a tunable charge injection barrier height. This behavior should be generally found in other metal/halide perovskite interfaces as well.

DOI: 10.1103/PhysRevMaterials.7.065405

I. INTRODUCTION

Recently, photovoltaics (PV) made with organometal halide perovskites have reached an efficiency above 25% [1], which rivals the efficiency of single crystal silicon cells. Despite the high efficiency, halide perovskite crystals contain a high concentration of point defects that are mobile at room temperature [2–6]. Because these defects can migrate back and forth under typical device operation conditions, the performance of perovskite PVs depends heavily on the precondition of the device, e.g., whether the device has been kept in the dark or was exposed to light [7–9], or whether the device has been operated at the reverse-bias condition [10]. The segregation of ionic defects not only changes the electric potential within the perovskite layer [11–13], it also modifies the local doping [14,15] and generates trapping sites for free carriers [16–22]. To further complicate the problem, the rate of defect migration can be enhanced by light illumination [23–31]. Understanding how the defect migration would affect the device performance is a very complex issue, but a thorough understanding is essential for mitigating various performance instabilities. On the other hand, the ease of defect migration and the strong defect-electron interaction can provide mechanisms for developing switchable devices.

The effect of defect migration and segregation on electron transport is often understood by modeling the current-voltage characteristic of PV devices operated under different conditions [11–13]. Although device modeling successfully captures some important observations such as the hysteresis found in the current-voltage measurement, it is difficult to untangle a variety of microscopic interactions between defects and charges. Very often, device modeling requires other independent measurements, such as diffusivities of various ionic defects, to justify or refine assumptions used in the model. While defect migration of point defects can be measured by other material characterization approaches [21,24,32–34], these methods generally do not capture how charged defect segregation can influence electron transport. Hence, there is a critical need for developing experimental tools that can unveil the correlation between ion migration and electron transport. Recently, by interfacing graphene with halide perovskites, we have used graphene as an electric field sensor to probe carrier trapping within the perovskite layer [15,35]. Combining with femtosecond (fs) pulsed laser excitations, we can further measure the electron transport time across the perovskite layer to the graphene electrode [35,36]. This work further advances this method by sandwiching the perovskite layer with a graphene electrode and a back gate. This capacitor structure allows us to control the direction and magnitude of the applied electric field across the perovskite layer by varying the back-gate voltage. This controllable electric field can drive ion migration. At the same time, the graphene sensor can probe ion segregation in the perovskite layer, and electron transfer between graphene and perovskite.

Using this approach, we find that methylammonium lead iodide ($MAPbI_3$), the commonly used halide perovskite, can effectively shield the graphene from the electric field through the migration and segregation of ionic defects. The shielding capability diminishes with decreasing temperature, but it is enhanced under light illumination, which resembles

*wlchan@ku.edu

the light-enhanced defect migration behavior found in halide perovskites [23–31]. Interestingly, we find that a positive (negative) defect accumulation layer near the perovskite-graphene interface, often referred to as the Debye layer, can facilitate electron (hole) injection from the graphene electrode to the perovskite. We argue that the charge injection from the metal to the perovskite can be facilitated by the large band bending in the Debye layer [10,11], and/or deep electron traps induced by the interaction between ionic defects and electron carriers [16–19].

Because the polarity of the defect accumulation layer can be switched by the application of an electric field, our work demonstrates that the metal-perovskite junction can be switched from an electron-injecting to a hole-injecting junction, and vice versa, by flipping the direction of the applied electric field. In other words, the graphene-perovskite junction behaves like a switchable Schottky diode in which its conduction behavior depends on the precondition of the perovskite layer, i.e., the type of ionic defects that accumulate near the conductor/perovskite interface. This contrasts with typical metal-semiconductor junctions at which the charge injection behavior is predetermined by the interfacial band alignment, which cannot be tuned easily by an external electric field. This switchable injection behavior of the metal-perovskite junction can be useful for applications which require that the electrical conductivity depends on the previous status of the device, e.g., memristors used for neuromorphic computing [37].

II. EXPERIMENTAL METHODS

A. Sample preparation

The perovskite capacitor was made by spin coating a perovskite film on a 300-nm SiO_2/Si (heavily doped) wafer. Then, graphene was transferred on top of the perovskite film by using a dry transfer method that we developed previously [36,38]. The SiO_2/Si substrate was cleaned with methanol and acetone, followed by an ozone treatment for 15 min before the spin coating. The $CH_3NH_3PbI_3$ film was prepared by a one-step spin-coating method [35,36]. The lead iodide (Alfa Aesar, 99.9985%) and methylammonium iodide (Luminescence Technology, 99.5%), in a stoichiometric ratio, were dissolved in dimethylformamide (SigmaAldrich, 99.8%) with a 1 M concentration. The solution was stirred at 70 °C overnight prior to use. The perovskite film was coated on the SiO_2/Si substrate by spin coating at 3000 rpm for 30 s in a nitrogen-filled glove box. During the spin coating, chlorobenzene (Macron), which acted as an antisolvent, was dropped onto the film. Then, the perovskite film was heated sequentially at 60 °C (5 min), 80 °C (5 min), and 100 °C (10 min) on a hot plate to remove the residual solvent. For the graphene transfer, chemical vapor deposition (CVD)-grown graphene-on-Cu (purchased from Graphene Supermarket) was used. Graphene was dry transferred on top of the perovskite film by using a PET/silicone stamp. The detailed procedure was discussed in Refs. [36,38]. As shown in our previous work [36], this method allows us to transfer a continuous graphene with a size of ∼1 cm onto the perovskite without exposing the perovskite surface to any solution.

B. Graphene device measurement

To fabricate the graphene capacitor, the graphene channel was patterned by using a shadow mask and Ar-ion sputtering. A pair of Cu electrodes (the source and drain electrodes) were deposited on the graphene through another shadow mask. All these processes were done in an ultrahigh vacuum chamber with a base pressure of 10^{-9} Torr. The size of the graphene channel was 1 mm × 1 mm. A schematic diagram of the capacitor is shown in Fig. 1(a). After all fabrication steps, the sample was mounted in a high vacuum cryostat, and it was kept in the dark overnight before measurement. A tungsten-halogen light source (Thorlabs SLS201L) was used for light illumination. An intensity of 0.13 mW cm^{-2} was used. During the measurement, a +5 or −5 V back-gate voltage (V_g) was applied to the highly doped Si substrate. A source-drain voltage (V_{sd}) of 1 V was applied across the top two Cu electrodes on the graphene channel and the source-drain current (I_{sd}) through the graphene channel was measured by a Keysight 34450A digital multimeter.

III. RESULTS AND DISCUSSION

A. Graphene as a charge sensor

To illustrate the working principle of the graphene charge sensor, we first highlight some previous results obtained from the perovskite/graphene/SiO_2/Si transistor, which is a commonly studied device structure. Unlike the perovskite capacitor, in the perovskite/graphene transistor, the perovskite film is not sandwiched between the back gate and the graphene [inset in Fig. 1(b)]. Hence, the electric field generated by the SiO_2/Si gate is shield by the graphene and does not extend into the perovskite film. Moreover, the graphene is located between the back gate and the perovskite. Therefore, its conductivity can be controlled independently by either using a back-gate voltage (electrical doping) or by exciting the perovskite optically (optical doping).

Unlike typical metallic conductors, the graphene conductivity is very sensitive to charge doping because of the low density of states (DOS) near the Fermi level (E_f) [39,40]. This unique property can be observed readily by doping the graphene using a Si/SiO_2 back gate in the perovskite/graphene transistor. Figure 1(b) shows the current passing through the graphene channel (I_{sd}) as a function of the back-gate voltage (V_g). When V_g is positive (negative), the graphene is doped with additional electrons (holes), which shifts the E_f up (down) with respect to the Dirac point (E_D), resulting in a change in its conductivity. The point at which the I_{sd} is minimum [labeled by a vertical bar in Fig. 1(b)] corresponds to $E_f = E_D$. Because the Dirac point is reached by applying a positive V_g, the as-prepared graphene in our lab is slightly p doped. Furthermore, by illuminating the sample with light, electrons are trapped in the perovskite layer; they dope the graphene with additional holes through capacitive coupling [35,36,41]. This additional p doping induced by light can be seen by the shifting of the Dirac point to the right [red arrow in Fig. 1(b)].

An I_{sd}-V_g curve for the graphene capacitor is shown in Fig. 1(c). For the capacitor device, as we will show, the I_{sd} changes with time after the V_g is switched on. On this plot,

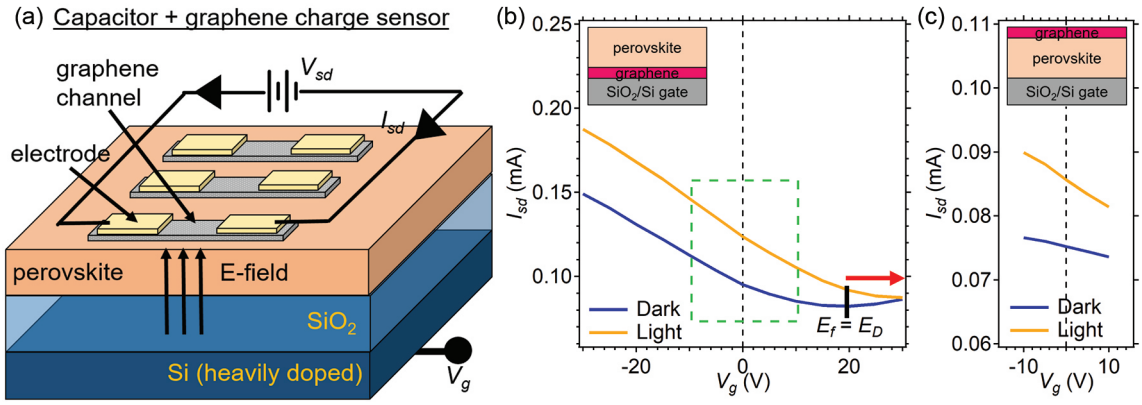

FIG. 1. (a) A schematic diagram showing the capacitor device used in our experiment. Three identical capacitors can be fabricated on a single sample. The direction and magnitude of the applied electric field can be controlled by the back-gate voltage (V_g). The charge doping in graphene is probed by the change in the source-drain current (I_{sd}). (b) The I_{sd} as a function of V_g for a typical graphene/perovskite transistor. The graphene is initially p doped and the Fermi level (E_f) reaches the Dirac point (E_D) when a positive V_g is applied. Under light illumination (intensity $= 0.13\,\mathrm{mW\,cm^{-2}}$), the graphene is doped by additional holes, as shown by the shifting of the Dirac point to the right (red arrow). (c) The I_{sd} as a function of V_g for the graphene/perovskite capacitor shown in (a). For experiments performed on the capacitor device, a V_g with a magnitude smaller than 10 V is applied. In this regime, an increase (decrease) in the I_{sd} represents additional hole (electron) doping in graphene.

we use the I_{sd} taken immediately after the V_g is switched on. For all measurements on perovskite capacitors that we will present, a small V_g, either -5 or $+5$ V, is used. For small V_g [see the green dashed box in Fig. 1(b), and Fig. 1(c)], the response of I_{sd} to V_g is rather linear. Moreover, an increase (decrease) in I_{sd} represents the graphene channel is doped with additional holes (electrons). This information will be used for understanding the data that we will present.

B. Ion segregation and charge injection

Now, we come back to the perovskite capacitor shown in Fig. 1(a). In this capacitor structure, an electric field can be applied through the perovskite layer by applying a V_g. The capacitor has two dielectric layers (SiO_2 and perovskite), which can be treated as two capacitors in series. Using standard equations for parallel plate capacitors in series, the potential drop across the perovskite layer V_p can be written as

$$V_p = V_g \frac{d_p \kappa_{SiO2}}{d_p \kappa_{SiO2} + d_{SiO2} \kappa_p}, \tag{1}$$

where κ_{SiO2} and κ_p are the static dielectric constants of SiO_2 and the perovskite, respectively. The thicknesses of the two layers are represented by d_{SiO2} and d_p. For our samples, $d_{SiO2} = 300$ nm and $d_p = 400$ nm [35,36]. In our measurements, a V_g with a magnitude of 5 V is chosen. By using $\kappa_p = 24.1$ [12,42] and $\kappa_{SiO2} = 3.8$, we got $V_p = 0.87$ V. This potential drop is similar to the typical built-in potential in an operating perovskite PV cell [12]. The V_p can drive the segregation of ionic defects in the perovskite layer, which can further increase the effective κ_p. Therefore, the ion segregation can cause the equivalent capacitance C_{eq} to increase with time. This effect will be accounted for when we estimate the number of injected charges in the later discussion. The temporal change of the equivalent capacitance C_{eq} and, hence, κ_p can be probed by measuring the number of charges stored in the graphene (one of the capacitor plates), which can in turn be monitored by measuring the change in the source-drain current (ΔI_{sd}) of the graphene channel as a function of time.

Figure 2(a) shows ΔI_{sd} as a function of time. At $t < 0$ s, no back-gate voltage is applied. We use $t = 0$ s as the reference point, where ΔI_{sd} ($t = 0$) is set to zero. At $t > 0$, a V_g equal to $+5$ V is applied. I_{sd} decreases ($\Delta I_{sd} < 0$) instantaneously after the back-gate voltage is switched on [arrow 1 in Fig. 2(a)]. This is expected because a positive V_g dopes the graphene channel with additional electrons [Fig. 2(c)], which decreases I_{sd}. When a positive V_g is applied, the electric field is pointing toward the graphene. Hence, positive (negative) ionic defects drift toward (away from) the graphene, which causes defect segregation [Fig. 2(d)]. The segregation of charged defects essentially increases the dielectric constant κ_p of the perovskite layer. This in turn should increase the C_{eq} and, hence, the number of charges stored in the graphene as shown in Fig. 2(d). As a result, the magnitude of ΔI_{sd} should increase as well. However, instead of increasing with time, interestingly, $|\Delta I_{sd}|$ decreases with time [arrow 2 in Fig. 2(a)]. This observation indicates a reduction in the number of doped electrons in the graphene. This reduction can occur if electrons in the graphene are injected into the perovskite as shown schematically in Fig. 2(e). In other words, the perovskite layer no longer behaves like a pure dielectric layer, but the electron injection from graphene to perovskite makes the perovskite behave like a part of the conducting plate of the capacitor. The number of electrons in graphene is reduced by the number of injected charges [Fig. 2(e)]. Indeed, for a parallel plate capacitor, positive charges on one side must be balanced by negative charges on the opposite side. Hence, the charge in the Si back gate (Q_{Si}), graphene (Q_{gr}), and the injected charge (Q_{inj}) can be related by

$$Q_{Si} = -(Q_{gr} + Q_{inj}). \tag{2}$$

The presence of the electron injection from graphene to perovskite is further supported by the overshooting of the

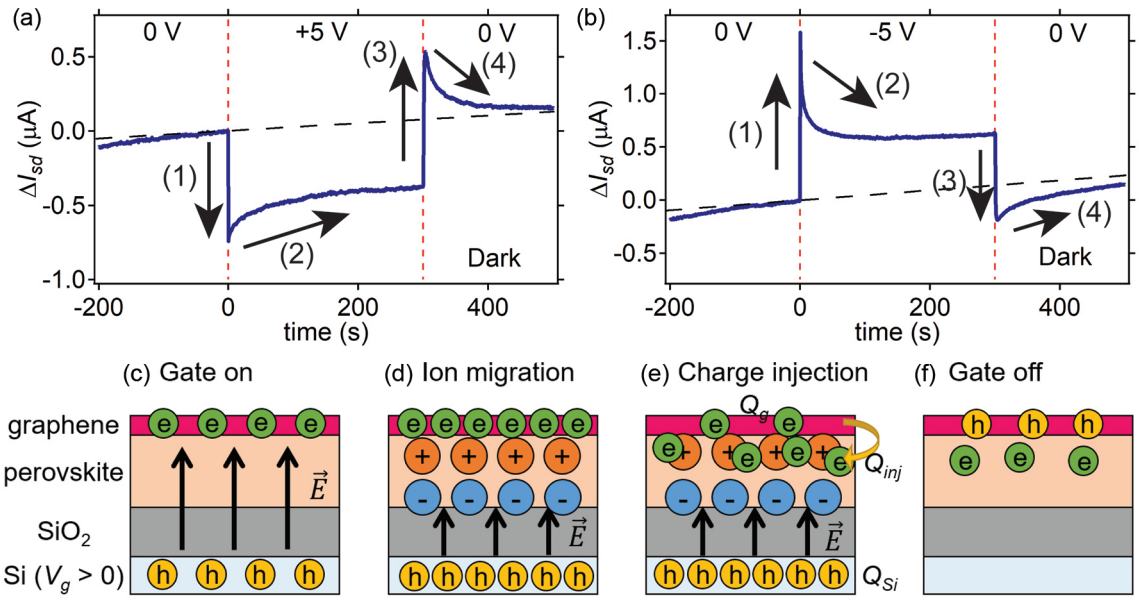

FIG. 2. (a), (b) The temporal change of the source-drain current (ΔI_{sd}) when the gate voltage (V_g) is switched on (at $t = 0$ s) and off (at $t = 300$ s). A V_g equal to +5 and −5 V was used for the measurement shown in (a), (b), respectively. The sample was kept in the dark during the measurement. (c)–(f) Schematics showing processes occurring in perovskite and graphene when a positive V_g is switched on and off. (c) When the V_g is first switched on, the graphene is doped by electrons due to the applied electric field. (d) Ion migration and segregation increase the capacitance, which should increase the amount of electron doping in graphene. (e) Electron injection from graphene to perovskite can reduce the doping in graphene, which leads to relaxation of the signal—see arrow 2 in (a). (f) Immediately after the V_g is switched off, injected electrons remain trapped in the perovskite. The trapped electrons induce hole doping in the graphene, which causes the overshooting of the signal above the baseline—see arrow 3 in (a).

ΔI_{sd} signal above the baseline when the V_g is switched off. In Fig. 2(a), V_g is switched off at $t = 500$ s [arrow 3 in Fig. 2(a)]. Instead of returning to the baseline, ΔI_{sd} becomes positive, which indicates that the graphene is now doped with additional holes. Because the V_g is switched off, the hole doping must be induced by electrons trapped in the perovskite layer as shown schematically in Fig. 2(f). These trapped electrons can eventually transfer back to the graphene, which causes ΔI_{sd} to restore gradually to the baseline [arrow 4 in Fig. 2(a)]. The same experiment is also done with a negative gate voltage ($V_g = -5$ V) and the data are shown in Fig. 2(b). Other than a change in the sign of ΔI_{sd}, very similar behaviors as compared to that obtained with a positive V_g are observed. We note that for $V_g < 0$, negatively charged defects are segregated near the graphene. Moreover, holes instead of electrons are injected from graphene to perovskite as the signal relaxes [arrow 2 in Fig. 2(b)].

To quantify the ratio of Q_{inj} and Q_{Si}, i.e., the number of injected charges relative to the total charges stored in the Si back gate, we define the percentage of signal relaxation (P) as

$$P = \frac{|\Delta I_{sd}(t_0)| - |\Delta I_{sd}(300\ \text{s})|}{|\Delta I_{sd}(t_0)|}, \tag{3}$$

where $|\Delta I_{sd}(t_0)|$ is the signal right after the V_g is switched on and $|\Delta I_{sd}(300\ \text{s})|$ is the signal after the V_g is switched on for ~ 300 s. At t_0, the signal is yet to relax and the number of charges in the graphene is equal to the number of charges in the back gate [Fig. 2(d)]. Hence, $|\Delta I_{sd}(t_0)|$ is proportional to Q_{Si}. After the charge injection, the residual signal $|\Delta I_{sd}(300\ \text{s})|$ is proportional to the number of charges remaining in the graphene [Fig. 2(e)]. It can be seen from Eq. (2) that the numerator in Eq. (3) is proportional to Q_{inj}. Therefore, P can also be written as

$$P = -Q_{inj}/Q_{Si}. \tag{4}$$

Because Q_{Si} is simply equal to $C_{eq}V_g$, we can estimate the number of injected charges by the P obtained from the measurement. We note that C_{eq} is increased by the defect segregation because the defect segregation should increase κ_p. However, because κ_{SiO2} is much smaller than κ_p, the value of C_{eq} is dominated by the capacitance of the SiO_2 layer. For example, if we increase κ_p from 24.1 to ∞, C_{eq} (for a capacitor area $A = 1\ \text{mm}^2$) only increases from 93 to 112 pF. For the data shown in Fig. 2, $P \sim 0.6$. Using Eq. (4), Q_{inj} and, hence, the area density of injected electrons/holes, can be found to be in the range of 1.75×10^{11}–2.1×10^{11} cm^{-2} (for $24.1 < \kappa_p < \infty$). We will correlate the injected charge density with the defect density in the perovskite in a later discussion.

In our measurements, the graphene does not directly probe the density of segregated ions because of the presence of the electron/hole injection from graphene to perovskite. Nevertheless, our measurement indicates that both electrons and holes can be injected effectively from graphene to perovskite because signal relaxation [arrow 2 in Figs. 2(a) and 2(b)] is observed for both positive and negative V_g. A detailed review on the physics of charge injection from a metal to a semiconductor can be found in Ref. [43]. Here, we note that the observation of the effective injection for both electrons and holes is rather surprising. This is because for electron injection from a conductor to a semiconductor to occur, E_f of the metal needs to be located near the conduction band minima (CBM) of the semiconductor, which results in a large Schottky

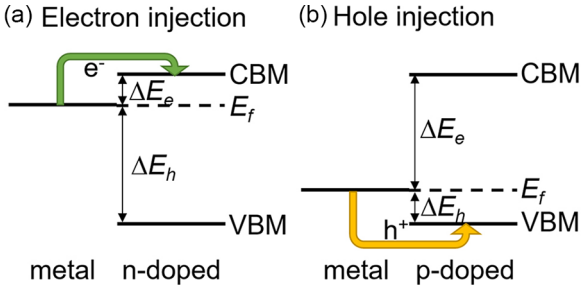

FIG. 3. (a) When a metal is interfaced with a n-type semiconductor, the Fermi level (E_f) is located close to the CBM, which can favor the injection of electrons into the perovskite (green arrow). (b) On the other hand, when the metal is interfaced with a p-type semiconductor, hole injection is favored (yellow arrow).

barrier for hole injection [Fig. 3(a)]. On the other hand, for the effective hole injection, E_f of the metal needs to be located close to the valence band maxima (VBM), which results in a large Schottky barrier for electron injection [Fig. 3(b)]. Hence, effective electron and hole injections from a metal to a semiconductor are usually mutually exclusive. It is rather anormal that both electron and hole injections can occur at a single metal/semiconductor interface. We attribute this bipolar charge injection behavior to the reversible defect segregation within the perovskite film. Defect segregation near the perovskite/graphene interface can produce defect states within the band gap. Moreover, ion segregation can produce a large band bending in the thin defect accumulation layer near the interface. As we will discuss, both factors would contribute to the observed bipolar electron/hole injection behavior. Before we discuss the charge injection mechanism, we will present data from experiments done at different temperatures and under light illumination.

C. Ion migration under light illumination and at low temperatures

In halide perovskites, it is known that the rate of defect migration can be enhanced by light illumination [23–30]. Therefore, the same measurement described in Fig. 2 is repeated except that the sample is now illuminated by a white light source with an intensity of 0.13 mW cm^{-2}. From previous works, it is known that light illumination can dope the graphene with holes as photoexcited electrons are preferentially trapped in perovskite [35,41]. The photodoping is manifested by the horizontal shift of the $I_{sd}-V_g$ curve shown in Fig. 1(b). For measurements done under light illumination, the sample is illuminated at a constant light intensity for at least 1 h prior to the measurement. This procedure ensures that I_{sd} becomes steady before the V_g is applied. Results obtained with positive and negative V_g are shown in Fig. 4. The dynamics of the signal relaxation under light illumination, after the V_g is switched on/off, is very similar to that observed in the dark (Fig. 2) expect that the extent of the relaxation is slightly more pronounced, i.e., a slightly larger P. The similarity between results obtained under light illumination and in the dark show that photocarriers alone cannot produce the observed behavior as no photocarrier is generated in the dark. On the other hand, the signal relaxation can still be

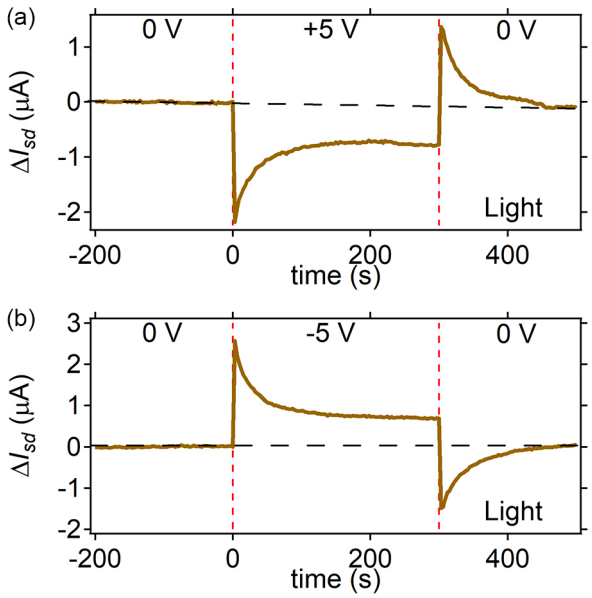

FIG. 4. The temporal change of the source-drain current (ΔI_{sd}) when the gate voltage (V_g) is switched on (at $t = 0$ s) and off (at $t = 300$ s). A V_g equal to +5 and −5 V was used for the measurement shown in (a), (b), respectively. During the measurement, the sample was illuminated by a white light source with an intensity of 0.13 mW cm^{-2}.

explained by electron/hole injection from graphene to perovskite as discussed earlier. At room temperature, light illumination does not significantly affect the dynamics of ΔI_{sd}. However, we found that the effect from the light illumination becomes much more apparent at low temperatures.

Figure 5 shows the temporal change of ΔI_{sd} at low temperatures as the V_g is switched on and off. Different curves are offset in the y axis for clarity. For all measurements, a rather symmetric flip in the ΔI_{sd} signal can be observed when the sign of V_g is changed. However, in the dark [Figs. 5(a) and 5(b)], we do not observe much signal relaxation for most temperatures after the V_g is switched on, i.e., a small P. Hence, electron and hole injections from graphene to perovskite diminish at low temperatures. Similarly, as the temperature is lowered, a very small overshooting of ΔI_{sd} above/below the baseline is observed immediately after the V_g is switched off, which is consistent with a smaller number of charges injected from graphene to perovskite. Results in Figs. 5(a) and 5(b) show that the charge injection process is significantly inhibited at low temperatures when the sample is kept in the dark.

On the other hand, the signal relaxation is rather pronounced even at low temperatures when the sample is illuminated by light. Figures 5(c) and 5(d) show the data collected under light illumination with positive and negative V_g, respectively. For a temperature as low as 100 K, significant signal relaxation and overshooting can still be observed, indicating that the charge injection can occur at much lower temperatures under light illumination. The signal relaxation and overshooting begin to diminish when the temperature is below 100 K. Figure 6 shows the portion of the relaxed signal [P in Eq. (3)] as a function of the temperature. As discussed earlier, the area density of injected carriers can be calculated

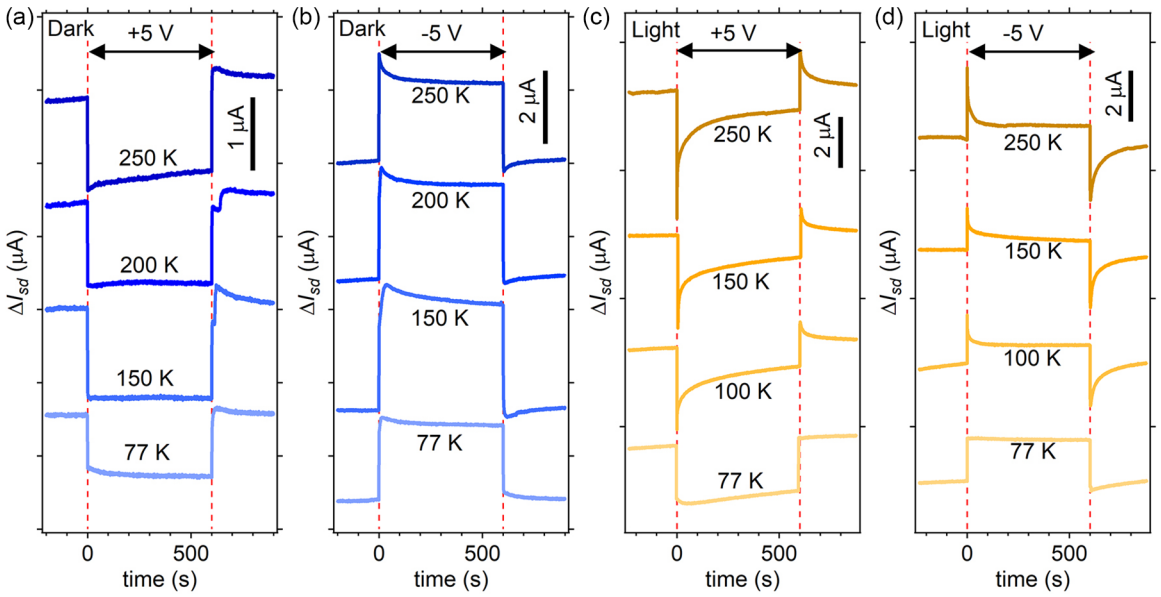

FIG. 5. The temporal response of the source-drain current (ΔI_{sd}) at different temperatures. The experimental conditions used were (a) dark, $V_g = 5$ V; (b) dark, $V_g = -5$ V; (c) light, $V_g = 5$ V; (d) light, $V_g = -5$ V. Curves are offset vertically for clarity. The vertical bar shows the scale for the current change.

from P, which is shown on the right axis in Fig. 6. When the sample is kept in the dark, the number of injected carriers drops significantly when the temperature is less than 250 K. By contrast, under light illumination, the number of injected carriers remains large until the temperature is lower than 100 K. This observation is consistent with the light-enhanced defect migration observed in halide perovskites. For example, it has been reported that the activation energy for defect migration decreases from 0.5 eV (in the dark) to 0.15 eV (under light illumination) [23]. Hence, the defect migration can only be deactivated at a much lower temperature when the sample is illuminated by light.

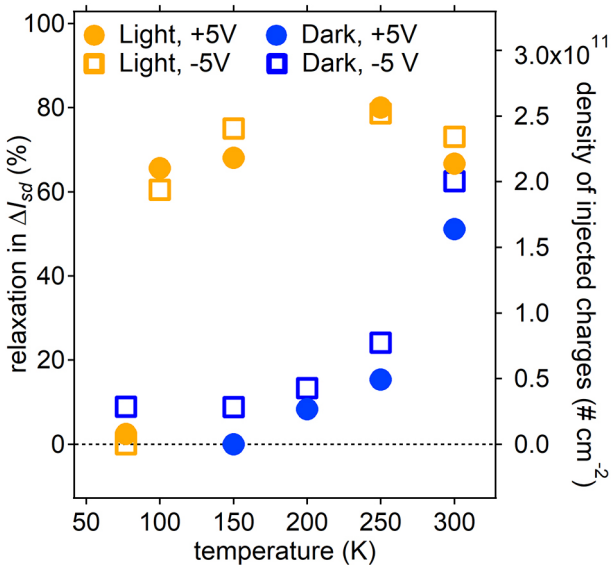

FIG. 6. The portion of relaxed signal [as defined in Eq. (3)] as a function of the temperature. The axis on the right shows the area density of injected carriers. When the sample is kept in the light, the charge injection can only be deactivated at a much lower temperature.

D. Charge injection facilitated by defect segregation

To understand how the charge injection would be facilitated by ion segregation, we note that ion segregation under an external field will build up two oppositely charged ionic layers on the two sides of the perovskite film. The two charged layers are known as Debye's layers [12]. Electrostatically, these Debye layers can induce a large band bending near the interface and shield the rest of the perovskite film from the applied electric field. Hence, the potential drop will be concentrated in the Debye layers. If the bending is large enough, the band bending associated with a positive (negative) ionic defect layer can facilitate electron (hole) injection through tunneling [10,11]. Such injection mechanism was proposed to occur in perovskite PVs under a reverse bias condition [10]. A schematic diagram illustrating ionic defect segregation, band bending, and injection through tunneling is shown in Fig. 7(a). The diagram is drawn for $V_g < 0$. At first sight, this tunneling mechanism would explain the experimental observation; i.e.,

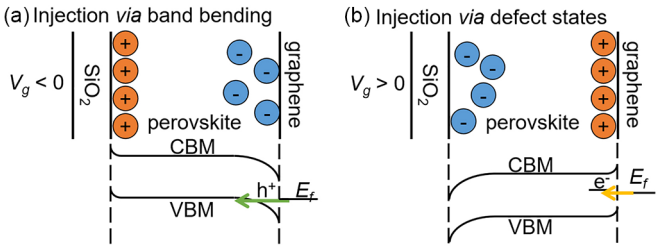

FIG. 7. Schematic diagrams showing how the ion segregation can induce charge injection from graphene to perovskite through (a) tunneling, and (b) defect states.

a positive (negative) Debye layer can facilitate electron (hole) injection from graphene. However, as pointed out in previous device modeling works [11], the total potential drop across the perovskite layer is unevenly distributed between the two defect accumulation layers because the positively charged defect, iodide vacancy (V_I), is much more mobile than its negative counterparts, such as MA vacancy (V_{MA}) and iodide interstitial (I_i) [44]. The difference in the defect mobility will make the V_I accumulation layer much thinner than its negative counterpart. As the magnitude of band bending is roughly proportional to the thickness of the Debye layer, the band bending in the V_I accumulation layer should be rather small.

In our capacitor, the total potential drop across the perovskite layer, V_p, [Eq. (1)], is 0.87 V. Previous modeling works suggest the thicknesses of the V_I accumulation and V_I depletion layers are 6 and 84 nm, respectively [11]. Assuming the magnitude of the band bending in each Debye layer is proportional to its thickness, and the sum of the band bending is equal to V_p, we estimate that the magnitude of band bending in the V_I accumulation layer is only ~ 0.06 eV. On the other hand, the band bending in the negative V_I depletion layer is much larger (0.81 eV). This asymmetry in the magnitude of band bending would favor the hole injection when a negative V_g is applied, but not the electron injection when a positive V_g is applied. However, in our experiment, very similar charge injection behavior is observed for both positive and negative V_g. Therefore, we argue that other mechanisms are present to facilitate the charge injection, especially for the electron injection at positive V_g.

When a positive V_g is applied, a V_I accumulation layer is built up near the graphene. Normally, V_I defects produce shallow trap states close to the CBM [45]. However, some theoretical works have shown that the V_I defect switches to a deep electron trap when the defect captures an additional electron, which distorts the surrounding lattice in a process known as Pb-Pb dimer formation [19,22,46–49]. Although this Pb-Pb dimer mechanism has been disputed by other simulations when more accurate hybrid functionals are used [18,50], simulations done with hybrid functionals do not preclude the formation of Pb-Pb dimers at the surface or in a region where V_I defects are clustered [17]. Our recent photoemission spectroscopy work [15] also provides experimental evidence for the Pb-Pb dimer formation at the surface of the $MAPbI_3$. Pb-Pb dimer formation can produce deep trap states. As illustrated schematically in Fig. 7(b), these traps states can be much closer to the Fermi level of graphene, which can facilitate the electron injection from graphene to perovskite. Hence, formation of deep electron traps, originated from defect-electron interaction, in the defect accumulation layer can serve as an additional mechanism to facilitate the electron injection from graphene to perovskite.

Finally, for either the tunneling [Fig. 7(a)] or the deep trap [Fig. 7(b)] mechanism, the number of injected electrons/holes should roughly balance the number of charged defects in the defect accumulation layer. Earlier, we showed that the area density of the injected electrons/holes is around 2×10^{11} cm^{-2}. Our perovskite film is 400 nm thick. If all defects in the film are accumulated at the Debye layer, the defect density in the perovskite film is $\sim 5\times10^{15}$ cm^{-3}. However, not all defects need to be segregated at the Debye layer because the defect segregation stops once the electric field generated from the back gate is shielded by the Debye layer. Therefore, the calculated density should be treated as the lower limit of defect density that is needed to produce the observed charge injection behavior. This lower limit is consistent with previous works, which suggest that the defect density of typical polycrystalline $MAPbI_3$ films is in the range of 10^{16}–10^{18} cm^{-3} [11,12]. In other words, because the defect density of polycrystalline halide perovskite films is typically larger than 10^{16} cm^{-3}, this large defect density is more than sufficient to support the charge injection behavior induced by defect segregation as observed in our experiment.

IV. CONCLUSION

In this work, a graphene/perovskite/SiO_2/highly doped Si capacitor is used to study the correlation between the defect segregation in the perovskite layer and the electron/hole injection behavior at the graphene/perovskite junction. When an external electric field is applied to the perovskite layer through an electrostatic gate, migration and segregation of ionic defects can occur. The defect segregation in the perovskite layer can effectively shield the graphene from the applied electric field, as seen by the rapid decay of the ΔI_{sd} signal. This behavior is akin to the behavior observed in perovskite PVs, in which ion migration and segregation can mostly shield the built-in electric field inside the perovskite film [51,52].

Interestingly, effective electron (hole) injection from the graphene to the perovskite layer can occur when positive (negative) ionic defects accumulate near the graphene electrode. The charge injection can be facilitated by the band bending induced by charged defects inside the Debye layer and deep traps created by carrier-defect interactions. Because the polarity of the Debye layer can be reversed by changing the direction of the applied electric field, the graphene/perovskite junction can be switched from a junction with a small Schottky barrier for electron injection to a junction with a small Schottky barrier for hole injection, and vice versa, by the application of an external electric field.

ACKNOWLEDGMENTS

W.-L.C. acknowledges the support by U.S. National Science Foundation Grant No. DMR-2109979 and the support by the University of Kansas General Research Fund Allocation No. 2151080. G.A. acknowledges the support provided by the Deanship of Scientific Research, Vice Presidency for Graduate Studies and Scientific Research, King Faisal University, Saudi Arabia (Grant No. 3154).

[1] H. Min, D. Lee, J. Kim, G. Kim, K. S. Lee, J. Kim, M. J. Paik, Y. K. Kim, K. S. Kim, M. G. Kim, T. J. Shin, and S. I. Seok, Perovskite solar cells with atomically coherent interlayers on SnO_2 electrodes, Nature (London) **598**, 444 (2021).

[2] Z. G. Xiao, Y. B. Yuan, Y. C. Shao, Q. Wang, Q. F. Dong, C. Bi, P. Sharma, A. Gruverman, and J. S. Huang, Giant switchable photovoltaic effect in organometal trihalide perovskite devices, Nat. Mater. **14**, 193 (2015).

[3] W. Tress, Metal halide perovskites as mixed electronic-ionic conductors: Challenges and opportunities—from hysteresis to memristivity, J. Phys. Chem. Lett. **8**, 3106 (2017).

[4] A. Walsh and S. D. Stranks, Taking control of ion transport in halide perovskite solar cells, ACS Energy Lett. **3**, 1983 (2018).

[5] D. A. Egger, A. M. Rappe, and L. Kronik, Hybrid organic-inorganic perovskites on the move, Acc. Chem. Res. **49**, 573 (2016).

[6] Y. Zhao, C. J. Liang, H. M. Zhang, D. Li, D. Tian, G. B. Li, X. P. Jing, W. G. Zhang, W. K. Xiao, Q. Liu, F. J. Zhang, and Z. Q. He, Anomalously large interface charge in polarity-switchable photovoltaic devices: An indication of mobile ions in organic-inorganic halide perovskites, Energy Environ. Sci. **8**, 1256 (2015).

[7] K. Domanski, B. Roose, T. Matsui, M. Saliba, S. H. Turren-Cruz, J. P. Correa-Baena, C. R. Carmona, G. Richardson, J. M. Foster, F. De Angelis, J. M. Ball, A. Petrozza, N. Mine, M. K. Nazeeruddin, W. Tress, M. Gratzel, U. Steiner, A. Hagfeldt, and A. Abate, Migration of cations induces reversible performance losses over day/night cycling in perovskite solar cells, Energy Environ. Sci. **10**, 604 (2017).

[8] F. Z. Huang, L. C. Jiang, A. R. Pascoe, Y. F. Yan, U. Bach, L. Spiccia, and Y. B. Cheng, Fatigue behavior of planar $CH_3NH_3PbI_3$ perovskite solar cells revealed by light on/off diurnal cycling, Nano Energy **27**, 509 (2016).

[9] W. Nie, J. C. Blancon, A. J. Neukirch, K. Appavoo, H. Tsai, M. Chhowalla, M. A. Alam, M. Y. Sfeir, C. Katan, J. Even, S. Tretiak, J. J. Crochet, G. Gupta, and A. D. Mohite, Light-activated photocurrent degradation and self-healing in perovskite solar cells, Nat. Commun. **7**, 11574 (2016).

[10] A. R. Bowring, L. Bertoluzzi, B. C. O'Regan, and M. D. McGehee, Reverse bias behavior of halide perovskite solar cells, Adv. Energy Mater. **8**, 1702365 (2018).

[11] L. Bertoluzzi, C. C. Boyd, N. Rolston, J. X. Xu, R. Prasanna, B. C. O'Regan, and M. D. McGehee, Mobile ion concentration measurement and open-access band diagram simulation platform for halide perovskite solar cells, Joule **4**, 109 (2020).

[12] G. Richardson, S. E. J. O'Kane, R. G. Niemann, T. A. Peltola, J. M. Foster, P. J. Cameron, and A. B. Walker, Can slow-moving ions explain hysteresis in the current-voltage curves of perovskite solar cells?, Energy Environ. Sci. **9**, 1476 (2016).

[13] N. E. Courtier, J. M. Cave, J. M. Foster, A. B. Walker, and G. Richardson, How transport layer properties affect perovskite solar cell performance: Insights from a coupled charge transport/ion migration model, Energy Environ. Sci. **12**, 396 (2019).

[14] Q. Wang, Y. C. Shao, H. P. Xie, L. Lyu, X. L. Liu, Y. L. Gao, and J. S. Huang, Qualifying composition dependent p and n self-doping in $CH_3NH_3PbI_3$, Appl. Phys. Lett. **105**, 163508 (2014).

[15] G. Alkhalifah, A. D. Marshall, F. Rudayni, S. Wanigasekara, J. Z. Wu, and W. L. Chan, Defect-polaron and enormous light-induced Fermi-level shift at halide perovskite surface, J. Phys. Chem. Lett. **13**, 6711 (2022).

[16] X. X. Feng, B. Liu, Y. Y. Peng, C. X. Gu, X. Bai, M. Q. Long, M. Q. Cai, C. J. Tong, L. Y. Han, and J. L. Yang, Restricting the formation of Pb-Pb dimer via surface Pb site passivation for enhancing the light stability of perovskite, Small **18**, 2201831 (2022).

[17] L. H. Zhang and P. H. L. Sit, *Ab initio* study of the dynamics of electron trapping and detrapping processes in the $CH_3NH_3PbI_3$ perovskite, J. Mater. Chem. A **7**, 2135 (2019).

[18] D. Meggiolaro and F. De Angelis, First-principles modeling of defects in lead halide perovskites: Best practices and open issues, ACS Energy Lett. **3**, 2206 (2018).

[19] W. Li, Y. Y. Sun, L. Q. Li, Z. H. Zhou, J. F. Tang, and O. V. Prezhdo, Control of charge recombination in perovskites by oxidation state of halide vacancy, J. Am. Chem. Soc. **140**, 15753 (2018).

[20] T. Leijtens, G. E. Eperon, A. J. Barker, G. Grancini, W. Zhang, J. M. Ball, A. R. S. Kandada, H. J. Snaith, and A. Petrozza, Carrier trapping and recombination: The role of defect physics in enhancing the open circuit voltage of metal halide perovskite solar cells, Energy Environ. Sci. **9**, 3472 (2016).

[21] A. M. Tirmzi, R. P. Dwyer, T. Hanrath, and J. A. Marohn, Coupled slow and fast charge dynamics in cesium lead bromide perovskite, ACS Energy Lett. **2**, 488 (2017).

[22] J. Wang, X. M. Duan, and W. J. Yin, Photoinduced dynamic defects responsible for the giant, reversible, and bidirectional light-soaking effect in perovskite solar cells, J. Phys. Chem. Lett. **12**, 9328 (2021).

[23] J. Xing, Q. Wang, Q. F. Dong, Y. B. Yuan, Y. J. Fanga, and J. S. Huang, Ultrafast ion migration in hybrid perovskite polycrystalline thin films under light and suppression in single crystals, Phys. Chem. Chem. Phys. **18**, 30484 (2016).

[24] G. Y. Kim, A. Senocrate, T. Y. Yang, G. Gregori, M. Gratzel, and J. Maier, Large tunable photoeffect on ion conduction in halide perovskites and implications for photodecomposition, Nat. Mater. **17**, 445 (2018).

[25] A. J. Barker, A. Sadhanala, F. Deschler, M. Gandini, S. P. Senanayak, P. M. Pearce, E. Mosconi, A. J. Pearson, Y. Wu, A. R. S. Kandada, T. Leijtens, F. De Angelis, S. E. Dutton, A. Petrozza, and R. H. Friend, Defect-assisted photoinduced halide segregation in mixed-halide perovskite thin films, ACS Energy Lett. **2**, 1416 (2017).

[26] E. T. Hoke, D. J. Slotcavage, E. R. Dohner, A. R. Bowring, H. I. Karunadasa, and M. D. McGehee, Reversible photo-induced trap formation in mixed-halide hybrid perovskites for photovoltaics, Chem. Sci. **6**, 613 (2015).

[27] S. J. Yoon, S. Draguta, J. S. Manser, O. Sharia, W. F. Schneider, M. Kuno, and P. V. Kamat, Tracking iodide and bromide ion segregation in mixed halide lead perovskites during photoirradiation, ACS Energy Lett. **1**, 290 (2016).

[28] H. C. Zhang, X. Fu, Y. Tang, H. Wang, C. F. Zhang, W. W. Yu, X. Y. Wang, Y. Zhang, and M. Xiao, Phase segregation due to ion migration in all-inorganic mixed-halide perovskite nanocrystals, Nat. Commun. **10**, 1088 (2019).

[29] S. Draguta, O. Sharia, S. J. Yoon, M. C. Brennan, Y. V. Morozov, J. M. Manser, P. V. Kamat, W. F. Schneider, and M. Kuno, Rationalizing the light-induced phase separation of mixed halide organic-inorganic perovskites, Nat. Commun. **8**, 200 (2017).

[30] M. C. Brennan, S. Draguta, P. V. Kamat, and M. Kuno, Light-induced anion phase segregation in mixed halide perovskites, ACS Energy Lett. **3**, 204 (2018).

[31] A. D. Marshall, J. Acharya, G. Alkhalifah, B. Kattel, W. L. Chan, and J. Z. Wu, Probing the origin of light-enhanced ion

diffusion in halide perovskites, ACS Appl. Mater. Inter. **13**, 33609 (2021).

[32] Y. B. Yuan and J. S. Huang, Ion migration in organometal trihalide perovskite and its impact on photovoltaic efficiency and stability, Acc. Chem. Res. **49**, 286 (2016).

[33] M. H. Futscher and C. Deibel, Defect spectroscopy in halide perovskites is dominated by ionic rather than electronic defects, ACS Energy Lett. **7**, 140 (2022).

[34] J. T. DuBose, P. S. Mathew, J. S. Cho, M. Kuno, and P. V. Kamat, Modulation of photoinduced iodine expulsion in mixed halide perovskites with electrochemical bias, J. Phys. Chem. Lett. **12**, 2615 (2021).

[35] L. Qin, L. P. Wu, B. Kattel, C. H. Li, Y. Zhang, Y. B. Hou, J. Wu, and W. L. Chan, Using bulk heterojunctions and selective electron trapping to enhance the responsivity of perovskite-graphene photodetectors, Adv. Funct. Mater. **27**, 1704173 (2017).

[36] L. Qin, B. Kattel, T. R. Kafle, M. Alamri, M. Gong, M. Panth, Y. Hou, J. Wu, and W. L. Chan, Scalable graphene-on-organometal halide perovskite heterostructure fabricated by dry transfer, Adv. Mater. Interfaces **6**, 1801419 (2019).

[37] Y. J. Park and J. S. Lee, Metal halide perovskite-based memristors for emerging memory applications, J. Phys. Chem. Lett. **13**, 5638 (2022).

[38] S. Wanigasekara, K. Rijal, F. Rudayni, M. Panth, A. Shultz, J. Z. Wu, and W. L. Chan, Using an atomically thin layer of hexagonal boron nitride to separate bound charge-transfer excitons at organic interfaces, Phys. Rev. Appl. **18**, 014042 (2022).

[39] F. Bonaccorso, Z. Sun, T. Hasan, and A. C. Ferrari, Graphene photonics and optoelectronics, Nat. Photon. **4**, 611 (2010).

[40] F. H. L. Koppens, T. Mueller, P. Avouris, A. C. Ferrari, M. S. Vitiello, and M. Polini, Photodetectors based on graphene, other two-dimensional materials and hybrid systems, Nat. Nanotechnol. **9**, 780 (2014).

[41] Y. Lee, J. Kwon, E. Hwang, C. H. Ra, W. J. Yoo, J. H. Ahn, J. H. Park, and J. H. Cho, High-performance perovskite-graphene hybrid photodetector, Adv. Mater. **27**, 41 (2015).

[42] F. Brivio, K. T. Butler, A. Walsh, and M. van Schilfgaarde, Relativistic quasiparticle self-consistent electronic structure of hybrid halide perovskite photovoltaic absorbers, Phys. Rev. B **89**, 155204 (2014).

[43] R. T. Tung, The physics and chemistry of the Schottky barrier height, Appl. Phys. Rev. **1**, 011304 (2014).

[44] H. X. Wang, A. Guerrero, A. Bou, A. M. Al-Mayouf, and J. Bisquert, Kinetic and material properties of interfaces governing slow response and long timescale phenomena in perovskite solar cells, Energy Environ. Sci. **12**, 2054 (2019).

[45] W. J. Yin, T. T. Shi, and Y. F. Yan, Unusual defect physics in $CH_3NH_3PbI_3$ perovskite solar cell absorber, Appl. Phys. Lett. **104**, 063903 (2014).

[46] M. L. Agiorgousis, Y. Y. Sun, H. Zeng, and S. B. Zhang, Strong covalency-induced recombination centers in perovskite solar cell material $CH_3NH_3Pbl_3$, J. Am. Chem. Soc. **136**, 14570 (2014).

[47] C. J. Tong, L. Q. Li, L. M. Liu, and O. V. Prezhdo, Synergy between ion migration and charge carrier recombination in metal-halide perovskites, J. Am. Chem. Soc. **142**, 3060 (2020).

[48] J. Wang, W. Li, and W. J. Yin, Passivating detrimental DX centers in $CH_3NH_3PbI_3$ for reducing nonradiative recombination and elongating carrier lifetime, Adv. Mater. **32**, 1906115 (2020).

[49] Z. S. Zhang, L. Qiao, C. Mora-Perez, R. Long, and O. V. Prezhdo, Pb dimerization greatly accelerates charge losses in $MAPbI_3$: Time-domain *ab initio* analysis, J. Chem. Phys. **152**, 064707 (2020).

[50] J. Kang, Effects of band edge positions on defect structure in lead halide perovskites: A case study on the Br vacancy in $CsPbBr_3$, Phys. Rev. Mater. **4**, 085405 (2020).

[51] P. Calado, A. M. Telford, D. Bryant, X. E. Li, J. Nelson, B. C. O'Regan, and P. R. F. Barnes, Evidence for ion migration in hybrid perovskite solar cells with minimal hysteresis, Nat. Commun. **7**, 13831 (2016).

[52] R. A. Belisle, W. H. Nguyen, A. R. Bowring, P. Calado, X. Li, S. J. C. Irvine, M. D. McGehee, P. R. F. Barnes, and B. C. O'Regan, Interpretation of inverted photocurrent transients in organic lead halide perovskite solar cells: Proof of the field screening by mobile ions and determination of the space charge layer widths, Energy Environ. Sci. **10**, 192 (2017).